

# Longitudinal Polarization of $\Lambda$ and $\bar{\Lambda}$ Hyperons in Lepton-Nucleon Deep-Inelastic Scattering

John Ellis<sup>1</sup>, Aram Kotzinian<sup>2,3,4</sup>, Dmitry Naumov<sup>2,5</sup>, and Mikhail Sapozhnikov<sup>2</sup>

<sup>1</sup> Theory Division, Physics Department, CERN, CH 1211 Geneva 23, Switzerland

<sup>2</sup> JINR, Dubna, Russia

<sup>3</sup> INFN, Torino, Italy

<sup>4</sup> Yerevan Physics Inst., Yerevan, Armenia

<sup>5</sup> INFN, Florence, Italy

Received: date / Revised version: date

CERN-PH-TH/2007-008

**Abstract.** We consider models for the spin transfers to  $\Lambda$  and  $\bar{\Lambda}$  hyperons produced in lepton-nucleon deep-inelastic scattering. We make predictions for longitudinal  $\Lambda$  and  $\bar{\Lambda}$  spin transfers for the COMPASS experiment and for HERA, and for the spin transfer to  $\Lambda$  hyperons produced at JLAB. We demonstrate that accurate measurements of the spin transfers to  $\Lambda$  and  $\bar{\Lambda}$  hyperons with COMPASS kinematics have the potential to probe the intrinsic strangeness in the nucleon. We show that a measurement of  $\bar{\Lambda}$  polarization could provide a clean probe of the spin transfer from  $\bar{s}$  quarks and provides a new possibility to measure the antistrange quark distribution function. COMPASS data in a domain of  $x$  that has not been studied previously will provide valuable extra information to fix models for the nucleon spin structure. The spin transfer to  $\bar{\Lambda}$  hyperons, which could be measured by the COMPASS experiment, would provide a new tool to distinguish between the SU(6) and Burkardt-Jaffe (BJ) models for baryon spin structure. In the case of the HERA electron-proton collider experiments with longitudinally-polarized electrons, the separation between the target and current fragmentation mechanisms is more clear. It provides a complementary probe of the strange quark distribution and helps distinguish between the SU(6) and BJ models for the  $\Lambda$  and  $\bar{\Lambda}$  spin structure. Finally, we show that the spin transfer to  $\Lambda$  hyperons measured in a JLAB experiment would be dominated by the spin transfer of the intrinsic polarized strangeness in the remnant nucleon, providing an independent way to check our model predictions.

**Key words.** lepton interactions, strange particles, polarization, spin transfer

**PACS.** 13.60.Rj Baryon production – 13.87.Fh Fragmentation into hadrons – 13.88.+e Polarization in interactions and scattering – 14.40.Ev Other strange mesons – 14.20.Jn Hyperons

## 1 Introduction

The origin of the nucleon spin remains a mystery. In a naive non-relativistic constituent quark model, one might have expected that quarks would carry essentially all the nucleon spin. However, measurements of axial-current matrix elements reduced this expectation to 60% even before the first polarized deep-inelastic scattering experiments were performed. These experiments have in fact discovered that the quarks carry only about 30% of the nucleon spin. The reasons for this discrepancy are still not clear, and it is also uncertain how the rest of the nucleon spin is divided between gluons and orbital angular momentum.

One model for the nucleon spin [1], motivated by simple soliton models, is that it is largely due to orbital angular momentum, with the quark and gluon contribution

each small. Another proposal [2,3,4] was that the naive quark contribution might have been reduced (in one particular renormalization scheme) by perturbative effects related to the axial-current anomaly in models with large gluon polarization, which would need to be counterbalanced by large and negative orbital angular momentum. A third proposal [5,6,7] has been that the net quark contribution might be suppressed by non-perturbative axial-current anomaly effects. A common feature of all these models is that the net strange quarks polarization  $\Delta s$  is expected to be negative, for either non-perturbative or (in the case of the second model) perturbative reasons.

Recent results on high- $p_T$  hadron production from HERMES [8], SMC [9] and COMPASS [10], charm production data from COMPASS [11] and particle-production asymmetries from RHIC [12] all indicate that the net gluon spin,  $\Delta G$ , is not large enough to suppress significantly the

---

*Correspondence to:* naumov@nusun.jinr.ru (D. Naumov)

net quark contribution to the nucleon spin via the proposed perturbative mechanism. However, the magnitude and sign of  $\Delta G$  are still relatively uncertain [13,14], and gluons may still contribute a large fraction of the proton spin. Neither are the present data on  $\Delta s$  yet conclusive. The data on inclusive polarized deep-inelastic scattering are interpreted as implying that the net strange polarization  $\Delta s \sim -0.08 \pm 0.02$  [13,15]. However, inclusive experiments provide only indirect evidence for this quantity, and the HERMES experiment has found no direct evidence for negative  $\Delta s$  in its analysis of particle-production asymmetries in polarized deep-inelastic scattering [16]. On the other hand, these data may not be in a kinematic regime where one can neglect subasymptotic corrections to the kinematic distributions, rendering this interpretation uncertain [17].

An alternative, direct probe of strange quark and antiquark polarization is provided by the polarization of  $\Lambda$  baryons and  $\bar{\Lambda}$  antibaryons produced in deep-inelastic scattering. Their longitudinal polarization is thought to be capable of ‘remembering’ the spin of the struck strange quark or antiquark, or the spin of the wounded nucleon remnant left behind in the target fragmentation region. This proposal [18] has been investigated in experiments on the deep-inelastic scattering of neutrinos, antineutrinos and charged leptons. To date, the most accurate measurement has been made by the NOMAD experiment, which found a large negative polarization of  $\Lambda$  baryons, increasing in the target fragmentation region [19,20,21,22]. This result is in qualitative agreement with the polarized-strangeness model [23,24], according to which a deep-inelastic neutrino collision would scatter preferentially off a valence quark with positive polarization along the exchange boson axis, leaving behind a target remnant containing a negatively polarized strange quark, whose state would be transferred statistically to  $\Lambda$  baryons produced in the target fragmentation region. This polarized-strangeness model has also been used to predict the net  $\Lambda$  polarization in the COMPASS experiment on polarized muon-nucleon scattering [25].

The purpose of this paper is to sharpen these predictions for the COMPASS experiment, to extend them to the  $\bar{\Lambda}$  spin transfer, to make new predictions for the HERA electron-proton collider with a polarized electron beam, and to extend the predictions to  $\Lambda$  production in a fixed-target experiment at JLAB.

We show that the polarization of  $\bar{\Lambda}$  hyperons provides a new possibility to probe the antistrange quark distribution in the nucleon. This is because the spin transfer to the  $\bar{\Lambda}$  depends completely on the antistrange quark distribution, whereas contributions from the other process to the  $\bar{\Lambda}$  spin transfer are negligible, so that the  $\bar{\Lambda}$  spin transfer depends only weakly on the associated theoretical uncertainties. On the other hand, accurate measurements of  $\bar{\Lambda}$  polarization could provide valuable information about  $\bar{\Lambda}$  spin structure. We show that the different schemes of  $\bar{\Lambda}$  spin structure result in markedly different predictions for the  $\bar{\Lambda}$  polarization, especially at large  $x_F$ .

At the HERA energy the target remnant and quark fragmentation mechanisms may be distinguished unambiguously, making possible more precise tests of the conjectured net negative polarization of the  $s$  quarks and antiquarks in the nucleon, via studies of  $\Lambda$  and  $\bar{\Lambda}$  production in both the remnant and current fragmentation regions.

At low energies, for conditions of a typical fixed-target JLAB experiment, we show that  $\Lambda$  production is dominated by diquark fragmentation, and extremely sensitive to the correlation between the polarization of the struck quark and that of the strange quark in the nucleon remnant.

The processes of spin transfer in the quark fragmentation to  $\Lambda$  and  $\bar{\Lambda}$  hyperons have been studied extensively in a number of theoretical models [26,27,28,29,30,31,32,33,34,35,36,37,38,39,40,41] for  $e^+e^-$  collisions and lepton nucleon deep-inelastic scattering processes. In this paper we consider also the contribution from the target nucleon remnant to the final  $\Lambda$  hyperon polarization.

This paper is organized as follows. In Section 2, we describe the model we use for hadron production in semi-inclusive deep-inelastic scattering, and describe various scenarios for the spin transfers to final-state  $\Lambda$  and  $\bar{\Lambda}$  hyperons. Section 3 presents results of the calculations for the different experimental conditions. Finally, we summarize our conclusions in Section 4.

## 2 Modelling the Hadronic Final State

We use common definitions for the kinematic variables:  $x, y$  are the standard deep-inelastic scaling variables and  $x_F$  is the Feynman variable defined as

$$x_F = \frac{2P_L^*}{W},$$

where  $P_L^*$  is the particle longitudinal momentum in the hadronic centre-of-mass system, whose invariant mass is denoted by  $W$ . This definition is approximate and valid only for high  $W$ . However it is commonly used for the lepton-hadron SIDIS in theoretical and experimental publications.

The negative range of  $x_F$  is often referred to as the target fragmentation region, and the positive range of  $x_F$  as the current fragmentation region. According to QCD factorization theorems, the hadron production in the current fragmentation region can be described as a convolution of quark distribution function in nucleon and quark fragmentation function. Similarly, one can suppose that particles in the target fragmentation region are originating from nucleon remnant fragmentation. We note, however, that the separation between these fragmentation mechanisms becomes effective only at very high centre-of-mass energies in lepton-nucleon scattering, so such terminology should be interpreted with care.

### 2.1 Fragmentation Model

We model the hadronization of quarks and target nucleon remnants into hadrons within the Lund string model, which

has been used successfully to describe many unpolarized phenomena, albeit with many free parameters that need to be tuned. Here we use the Lund model as implemented in the JETSET 7.4 [42, 43] code, with the string fragmentation parameters tuned by the NOMAD experiment [44]. These parameters describe well the yields of the strange hadrons  $\Lambda$ ,  $\bar{\Lambda}$ ,  $K_S^0$  and - what is important for our calculations - the relative contributions of  $\Lambda$  and  $\bar{\Lambda}$  hyperons produced from decays of heavier states ( $\Sigma^*$ ,  $\Sigma^0$ ,  $\Xi$  and their antiparticles) [19, 20, 45]. Deep-inelastic lepton-nucleon scattering is simulated using the LEPTO 6.1 [46] package, with parton distributions provided by the PDFLIB package [47].

We would like to mention two important improvements to the LEPTO 6.1 package that we implement here.

1. We incorporate lepton scattering off sea  $u$  and  $d$  quarks, which was not modelled in the LEPTO code, as was mentioned in [25]. It is very important because in the original LEPTO 6.1 the scattering over sea  $u, d$  quarks was simply treated in the same way as valence  $u, d$  quarks. When scattering occurs on the sea quark the target remnant is not a simple diquark. Obviously this changes a lot the final-state hadronization for charged leptons interactions because of small  $x$  dominance at higher energies.
2. In order to describe scattering on a nucleus, the LEPTO code treats its quark distributions as mixtures of proton and neutron quark distribution functions weighted by the relative numbers of protons and neutrons in the nucleus. This has the feature that, in the event sample so generated, the distributions of different quark flavours are independent of the type of target nucleon on which the scattering event takes place, and also of the final-state hadron selected in semi-inclusive reactions. We use here a different procedure which describes these reactions more correctly. For the production of any given hadron, we simulate separate samples of events produced on individual proton and neutron targets and combine these samples statistically to obtain the semi-inclusive cross section for any given hadron on a composite nuclear target. The improvement is important because the  $\Lambda$  polarization strongly depends on the type of nucleon scattered and the quark scattered. However LEPTO 6.1 mixes the quark density functions of protons and neutrons if one requires an “averaged nucleon” (like deuteron). This is good procedure for the DIS but not for SIDIS. For  $\Lambda$  production this will give wrong contributions of heavier states (like  $\Sigma^*$ ,  $\Sigma^0$  etc). This procedure also incorporates the correct final-state particle correlations.

## 2.2 Ranks in String Fragmentation

As preparation for the treatment of spin transfer to final-state  $\Lambda$  and  $\bar{\Lambda}$  hyperons, we introduced in [25] two hadronization ranks  $R_q$  and  $R_{qq}$ . The ranks  $R_q$  and  $R_{qq}$  are integers equal to the numerical ordering of the hadron from the quark and the opposite end, which we call the nucleon

target end <sup>1</sup>. Some examples of the assignments of these two ranks are shown in Fig. 1.

We often use in the following the terms of quark (target remnant) fragmentation for the case  $R_q < R_{qq}$  ( $R_{qq} < R_q$ ). However, one must always bear in mind that one is dealing with string hadronization, and not with independent fragmentation.

## 2.3 Models for Spin Transfer

The polarization of the interacting quark, denoted by  $P_q$ , is given by

$$P_q = P_B D(y), \quad (1)$$

where  $P_B$  is the charged-lepton longitudinal polarization, and  $D(y)$  is the depolarisation factor, in the leading order taken to be  $D(y) = \frac{1-(1-y)^2}{1+(1-y)^2}$ . Corrections to  $D(y)$  well parametrized for DIS are poorly known for SIDIS production of different hadrons.

We assume that there are two basic mechanisms for a baryon to be produced in a deep-inelastic process with longitudinal polarization, via spin transfer from the struck quark or from the target nucleon remnant. The  $\Lambda$  and  $\bar{\Lambda}$  hyperons may be produced either promptly or via the decays of heavier resonances such as  $\Sigma^*$ ,  $\Sigma^0$ ,  $\Xi$  and their antiparticles, which also transfer partially their polarization to the  $\Lambda$  or  $\bar{\Lambda}$ . We take both possibilities into account.

The spin transfer from the nucleon target remnant to the  $\Lambda$  and  $\bar{\Lambda}$  hyperons can be due to either polarization of the remnant diquark system (after the struck quark is removed from the nucleon) or possible sea polarization of quarks (and antiquarks) produced via intermediate string breaking, which then fragment into the baryon considered.

Following [25], we consider in the following two extreme cases for spin transfer to hyperons.

- **Model A:** Restrict spin transfer in (di-)quark fragmentation to hyperons with ( $R_{qq} = 1, R_q \neq 1$ )  $R_{qq} \neq 1, R_q = 1$ .
- **Model B:** Allow spin transfer in (di-)quark fragmentation to hyperons with ( $R_{qq} < R_q$ )  $R_{qq} > R_q$ .

The spin transfer in quark and diquark fragmentation is then calculated as follows.

### 2.3.1 Spin Transfer from the Struck Quark

The polarization of  $\Lambda$  and  $\bar{\Lambda}$  hyperons produced promptly or via the decay of a strange baryon  $Y$  in quark fragmentation is assumed to be related to the quark polarization  $P_q$  by:

$$\begin{aligned} P_\Lambda^q(Y) &= -C_\Lambda^q(Y) P_q, \\ P_{\bar{\Lambda}}^{\bar{q}}(\bar{Y}) &= -C_{\bar{\Lambda}}^{\bar{q}}(\bar{Y}) P_{\bar{q}}, \end{aligned} \quad (2)$$

<sup>1</sup> For example, for scattering on a valence quark, this end represents the remnant diquark of the nucleon, but it can also be a quark or antiquark, for details see [46].

where  $C_q^\Lambda(Y) = C_{\bar{q}}^{\bar{\Lambda}}(\bar{Y})$  are the corresponding spin-transfer coefficients. For the sake of simplicity we use the notation  $C_q^\Lambda(Y)$  for both  $\Lambda$  and  $\bar{\Lambda}$ .

We use two different models to calculate  $C_q^\Lambda(Y)$ . The first one is based on non-relativistic SU(6) wave functions, where the  $\Lambda$  ( $\bar{\Lambda}$ ) spin is carried only by its constituent  $s$  ( $\bar{s}$ ) quark. In this case, the promptly-produced  $\Lambda$  ( $\bar{\Lambda}$ ) hyperons could be polarized only in  $s$  ( $\bar{s}$ ) quark fragmentation. The second approach was suggested by Burkardt and Jaffe (BJ) [26], who assumed that the modification of the SU(6) spin decomposition discovered in the case of the nucleon exists also for other octet hyperons. The spin contents of all octet baryons within this approach were obtained in [34]. Table 1 summarizes the spin-correlation coefficients in the SU(6) and BJ models for both prompt  $\Lambda$  hyperons and octet and decuplet intermediate hyperons.

**Table 1.** Spin correlation coefficients in the SU(6) and BJ models.

$\Lambda$ 's parent	$C_u^\Lambda$		$C_d^\Lambda$		$C_s^\Lambda$	
	SU(6)	BJ	SU(6)	BJ	SU(6)	BJ
quark	0	-0.18	0	-0.18	1	0.63
$\Sigma^0$	-2/9	-0.12	-2/9	-0.12	1/9	0.15
$\Xi^0$	-0.15	0.07	0	0.05	0.6	-0.37
$\Xi^-$	0	0.05	-0.15	0.07	0.6	-0.37
$\Sigma^*$	5/9	-	5/9	-	5/9	-

In Model A the  $\Lambda$  and  $\bar{\Lambda}$  are polarized according to (2) if  $R_q = 1$  and  $R_{qq} \neq 1$ . In Model B the corresponding condition is  $R_q < R_{qq}$ . We assume that no spin transfer occurs if  $R_q = R_{qq}$ .

### 2.3.2 Spin Transfer from the Remnant Diquark

We parametrize a possible sea-quark polarization as a *correlation* between the polarization of the sea quark and that of the struck quark, described by the spin-correlation coefficients  $C_{sq}$ :

$$P_s = C_{sq} P_q, \quad (3)$$

where  $P_q$  and  $P_s$  are the polarizations of the initial struck quark and the strange quark. The values of the  $C_{sq}$  parameters (one for scattering on a valence quark, the other for scattering on a sea quark) were found in a fit to NOMAD data [25]:

#### Model A:

$$C_{sq_{val}} = -0.35 \pm 0.05, C_{sq_{sea}} = -0.95 \pm 0.05. \quad (4)$$

#### Model B:

$$C_{sq_{val}} = -0.25 \pm 0.05, C_{sq_{sea}} = 0.15 \pm 0.05.$$

We calculate as follows the polarizations of  $\Lambda$  hyperons produced in target remnant fragmentation:

$$\begin{aligned} P_A^{l,u}(\text{prompt}; N) &= P_A^{l,d}(\text{prompt}; N) = C_{sq} \cdot P_q, \\ P_A^{l,u}(\Sigma^0; p) &= P_A^{l,d}(\Sigma^0; n) = \frac{1}{3} \cdot \frac{2 + C_{sq}}{3 + 2C_{sq}} \cdot P_q, \\ P_A^{l,u}(\Sigma^{*0}; p) &= P_A^{l,d}(\Sigma^{*0}; n) = P_A^{l,d}(\Sigma^{*+}; p) = \\ P_A^{l,u}(\Sigma^{*-}; n) &= -\frac{5}{3} \cdot \frac{1 - C_{sq}}{3 - C_{sq}} \cdot P_q. \end{aligned} \quad (5)$$

The equations (5) are applicable only for  $\Lambda$  hyperons, because we assume that  $\bar{\Lambda}$  hyperons cannot acquire polarization from the nucleon remnant.

## 3 Predictions for Experiments

For the sake of comparison with experimental data with various beam polarizations, in what follows we present our results for the spin transfer as defined by

$$S \equiv \frac{P_{\Lambda(\bar{\Lambda})}}{P_B D(y)}. \quad (6)$$

Most of the calculations presented in this section have been performed for the COMPASS experimental conditions, namely deep-inelastic scattering of positive muons with an energy of 160 GeV and beam polarization  $P_b = -0.76$  on an isoscalar  ${}^6\text{LiD}$  target. We consider scattering on an unpolarized target, as appropriate for comparison with the first COMPASS experimental data analysis on spin transfer to  $\Lambda$  and  $\bar{\Lambda}$  [48]. We also provide our predictions for two other experimental cases: HERA  $e - p$  collisions ( $E_e = 27.5$  GeV,  $E_p = 820$  GeV) and JLAB fixed-target electron-proton scattering ( $E_e = 5.7$  GeV). In both cases, we assume an electron polarization  $P_b = -0.8$ . The standard deep-inelastic cut  $Q^2 > 1$  GeV<sup>2</sup> was imposed for these experimental conditions.

### 3.1 Characteristics of $\Lambda$ and $\bar{\Lambda}$ Production

In order to understand the spin transfer to hyperons, it is important first to clarify the relative roles of different mechanisms for  $\Lambda$  ( $\bar{\Lambda}$ ) production in deep-inelastic scattering.

In Fig. 2 we show the  $x_F$  distributions of  $\Lambda$  and  $\bar{\Lambda}$  hyperons produced at the COMPASS energy. The plots are shown for Model B, using the GRV98 parametrization [49] of the parton distribution functions and the SU(6) model for the  $\Lambda$  spin structure. However, similar trends are exhibited by Model A and other choices of the parton distribution functions and  $\Lambda$  spin structure.

One may conclude from Fig. 2 (left) that in all the  $x_F$  region the main contribution to  $\Lambda$  production is that due to diquark fragmentation (dash-dotted line). This dominance was to be expected in the target fragmentation region ( $x_F < 0$ ), but at the COMPASS energy the diquark



fragmentation is important even in the current fragmentation region ( $x_F > 0$ ).

As was also demonstrated previously [25], heavy hyperon decays are important sources of  $\Lambda$  production. In Fig. 2 the contribution from heavy hyperons produced from the target nucleon remnant (dashed line) and quark fragmentation (dotted line) are shown. The contribution from the fragmentation of  $u, d$  light quarks (dash-triple-dotted line) are considerably smaller than these two sources, especially at  $x_F < 0$ . The contribution from the  $s$ -quark fragmentation (long dashed line) increases at large and positive  $x_F$ . At  $x_F = 0.5-0.8$  it grows larger than the contribution from resonance decays, though it is still smaller than the contribution due to diquark fragmentation.

We now extend the discussion of [25] to  $\bar{\Lambda}$  production. Its  $x_F$  dependence is shown in Fig. 2 (right). One can see that diquark fragmentation (dash-dotted line) is dominant in the region of small  $x_F < 0.5$ . For  $\bar{\Lambda}$  production this statement means simply that the  $\bar{\Lambda}$  prefers to be formed near the diquark end of the corresponding string. It differs from the diquark fragmentation of  $\Lambda$ , as in that case the diquark could fragment directly to the hyperon, and therefore transfer its polarization to the hyperon. According to our assumptions, there is no spin transfer in diquark fragmentation to an antihyperon.

We also see that heavy hyperon decays (dashed line) are insignificant for  $\bar{\Lambda}$  production, whereas the contribution of  $\bar{s}$ -quark fragmentation (long dashed line) is more important for  $\bar{\Lambda}$ . At large  $x_F > 0.6$ , the  $\bar{\Lambda}$  are produced mainly from  $\bar{s}$  quarks. This contribution is larger than the diquark fragmentation, heavy hyperon decays or fragmentation from light quarks (dash-triple-dotted line). Thus, at the COMPASS energy,  $\bar{\Lambda}$  production may serve as a clean source of information about the antistrange sea of the nucleon, better than  $\Lambda$  production.

It is interesting that similar dependencies exist at the highest energy we consider, namely that of HERA. In Fig. 3 we show the  $x_F$  distributions of  $\Lambda$  and  $\bar{\Lambda}$  produced in DIS with HERA conditions. One can see that diquark fragmentation (dash-dotted line) still dominates, even at this HERA energy. The production of the  $\Lambda$  via heavy hyperon decays (dashed line) is important only in the region  $x_F < 0$ . The contribution from quark fragmentation in general, and from the strange quark in particular, is more clearly separated. The pronounced peak around  $x_F = 0$  is due to scattering on sea light and strange quarks. Even at HERA energy, diquark fragmentation makes the largest contribution to  $\Lambda$  production, but conditions for the study of different quark contributions to the  $\Lambda$  production are better than at lower energy. In the case of  $\bar{\Lambda}$  production, we see that the production from  $\bar{s}$  fragmentation is dominant at  $x_F > 0.5$ .

### 3.2 Spin Transfer for $\Lambda$ and $\bar{\Lambda}$

In Fig. 4 we show the spin transfers (6) to  $\Lambda$  and  $\bar{\Lambda}$  hyperons in the  $SU(6)$  scheme for model B, as functions of  $x_F$  at the COMPASS energy. The solid line in Fig. 4 corresponds to the full calculation, whereas the amount of spin

transfer without the contribution of the  $u, d$  quarks ( $\bar{u}, \bar{d}$  for  $\bar{\Lambda}$ ) is shown as the dotted line, and the spin transfer without the contribution of the  $s$  quarks is shown as the long-dashed line. The dashed line shows the spin transfer when we set  $C_{sq} = 0$  in (3).

The left panel of Fig. 4 clearly displays two main mechanisms of spin transfer to  $\Lambda$  hyperons: target nucleon remnant (at  $x_F < 0$ ) and current fragmentation. It is noteworthy that switching off the  $s$ -quark contribution removes completely the spin transfer for  $x_F > 0.2$ . In this region the polarization of the  $\Lambda$  is determined essentially by the scattering on  $s$  quarks. The contribution from the struck light quarks is small and opposite in sign from the positive spin transfer from the  $s$  quark (mainly due to the  $\Sigma^0$  resonance). Switching off the scattering on light quarks almost removes the spin transfer to  $\Lambda$  hyperons at negative  $x_F$  because in this case the production of  $\Lambda$  hyperons from the target nucleon remnant (and thus spin transfer via  $C_{sq}$ ) is significantly suppressed.

In the right panel of Fig. 4 the spin transfer to  $\bar{\Lambda}$  hyperons is shown. At positive  $x_F$  the spin transfer to  $\bar{\Lambda}$  is significantly larger than that to  $\Lambda$ . Moreover, *the spin transfer to the  $\bar{\Lambda}$  completely disappears when the  $\bar{s}$  contribution is switched off*. The contribution from the fragmentation of the light quarks is small. Therefore, almost all the spin transfer from the lepton to the  $\bar{\Lambda}$  hyperon is due to fragmentation of the antistrange quarks. Hence, one may expect that the  $\bar{\Lambda}$  spin transfer should be quite sensitive to the details of the antistrange quark distribution in the nucleon. In Sect. 3.3-3.6 we will study just to what extent this feature depends on the models considered.

Whilst the  $x_F$  distributions for the spin transfers to  $\Lambda$  and  $\bar{\Lambda}$  hyperons reflect largely the main spin-transfer mechanisms, we have also to keep in mind the  $x$  dependence of the spin transfer to  $\Lambda$  hyperons due to the different  $C_{sq}$  coefficients (4). Fig. 5 displays the spin transfers to  $\Lambda$  and  $\bar{\Lambda}$  hyperons for the COMPASS conditions as functions of  $x$  and  $x_F$ . In the left panel of Fig. 5 there are two visible regions with significant spin transfer to  $\Lambda$  hyperons. The first region is where  $x_F < 0$ , and the spin transfer from the target nucleon remnant is dominant, whereas the second region is where  $x_F > 0$ , and  $s$ -quark fragmentation dominates at small  $x$ .

Examining Fig. 5 for the  $\Lambda$  hyperon case, one can see that the  $x$  dependence of the spin transfer is different in different slices of the  $x_F$  variable, especially comparing the domains  $x_F < 0$  and  $x_F > 0$ . One must take this into account when comparing theory predictions with experimental data folded with real experimental acceptance.

In the right panel of Fig. 5 we show the spin transfer to  $\bar{\Lambda}$  hyperons, which is mainly due to  $\bar{s}$  fragmentation and has a simpler structure. This facilitates the investigation of the  $\bar{s}$  quark distribution using the spin transfer to  $\bar{\Lambda}$ .

In Fig. 6 we display the spin transfers to  $\Lambda$  and  $\bar{\Lambda}$  hyperons as functions of  $x$  and  $y$ . The calculations are made in the  $SU(6)$  model with the GRV98 parton density functions. We see that the model predicts small (or zero) spin transfer to  $\Lambda$  in the region  $x \sim 10^{-2}$ , which increases monotonously to  $S \sim 0.1$  at  $x \sim 10^{-1}$ . The  $x$  dependence

of the spin transfer to  $\bar{\Lambda}$  is different from that of the  $\Lambda$ , being quite constant in  $x$  around  $S \sim 0.05$ . The exact value of  $S$  depends on the theoretical option used. For instance, it is different in Models A and B, providing a good test for discriminating between them.

The  $y$  dependencies of the spin transfers to  $\Lambda$  and  $\bar{\Lambda}$  are also different, as shown in Fig. 6 (right) for Model B. The  $y$  dependence of the spin transfer to  $\bar{\Lambda}$  is quite constant, as it should be if the quark fragmentation mechanism of the  $\bar{\Lambda}$  production dominates. On the other hand, the  $y$  dependence of the spin transfer to  $\Lambda$  decreases with  $y$ , reflecting the role of the target remnant. It is interesting that dropping the contribution from the target remnant, i.e., assuming  $C_{sq} = 0$  (or considering only the region  $x_F > 0$ ), leads to the disappearance of the  $y$  dependence for  $\Lambda$ . It becomes almost constant with a spin-transfer value that is about a factor of two smaller.

### 3.3 Comparison between Models A and B

In Fig. 7 we compare the predictions of Models A and B for the  $x_F$ ,  $x$  and  $y$  distributions of the spin transfer to  $\Lambda$  and  $\bar{\Lambda}$  hyperons in the COMPASS experimental conditions.

It is worthwhile recalling that the free parameters of our models for the spin transfer from the intrinsic strangeness of the nucleon ( $C_{sq}^{val}$ ,  $C_{sq}^{sea}$ ) were tuned using data from the NOMAD experiment [19]. The COMPASS kinematics extends the  $x$  region to much lower values not accessible to NOMAD, where the two Models A and B differ significantly in their predictions. We recall also that the fit to the NOMAD data performed in [25] yielded negative correlation coefficients  $C_{sq_{val}}$ ,  $C_{sq_{sea}}$  for Model A, but negative  $C_{sq_{val}}$  and positive  $C_{sq_{sea}}$  for Model B, as can be seen in (4). Therefore, the two models diverge in their predictions at small  $x$  where the role of sea quarks is significant, as can be seen from the  $x$  dependence of the spin transfer to  $\Lambda$  hyperons shown in Fig. 7. This is reflected in the large difference between models A and B at negative  $x_F$ . A larger contribution to the spin transfer to  $\Lambda$  hyperons from resonances produced in the quark fragmentation is generally found in Model B. This is reflected in a smaller spin transfer at positive  $x_F$  in Model B, as compared to Model A.

Remarkably, in the case of  $\bar{\Lambda}$  polarization the predictions of Models A and B are nearly the same. This stability is due in part to a compensation of the primary spin transfer to the  $\bar{\Lambda}$  hyperons by antiresonance contributions. On the one hand, Model B allows more  $\bar{\Lambda}$  to be produced from quark fragmentation (and thus a higher spin transfer is expected on average), on the other hand it also increases the fraction of  $\bar{\Lambda}$  hyperons produced from antiresonance decays. These are dominated by  $\bar{\Sigma}^0$  decays that transfer the opposite polarization.

Thus, the  $\Lambda$  data could be used to discriminate between Models A and B. On the other hand, the predictions of the spin transfer to  $\bar{\Lambda}$  are robust and do not depend on the assumption about the spin-transfer assignment in a certain ranking scheme.

### 3.4 Sensitivity to the Strange Quark Parton Distributions

In Fig. 8 we show the spin transfers to the  $\Lambda$  and  $\bar{\Lambda}$  hyperons as calculated using the CTEQ5L set of parton distribution functions [50] for the COMPASS energy, enabling us to demonstrate the effects of different strange quark parton distributions. The GRV98 set is based on the assumption that there is no intrinsic nucleon strangeness and the strange sea is of pure perturbative origin. On the other hand, the CTEQ collaboration takes into account the dimuon data of the CCFR and NuTeV experiments [51,52]. As a result, the  $s(x)$  distribution of CCFR is larger than the GRV98 one by a factor of about two in the region  $x = 0.001 - 0.01$ . To show how this difference in  $x$ -dependence reflected in the  $x_F$  dependence we plot in Fig. 8 the spin transfers to the  $\Lambda$  and  $\bar{\Lambda}$  hyperons. It turns out that the CTEQ parton distribution results in larger spin transfer to both  $\Lambda$  and  $\bar{\Lambda}$ .

Therefore, precise measurements of the  $\bar{\Lambda}$  spin transfer could give useful information about the antistrange quark distribution, which could be complementary to the other inclusive deep-inelastic data, which is sensitive to the unpolarized sum  $s(x) + \bar{s}(x)$ .

In Fig. 9 we display our predictions for the spin transfer to the  $\Lambda$  and  $\bar{\Lambda}$  hyperons for the GRV98 and CTEQ5L sets of parton distributions as functions of  $x_F$  with HERA kinematics. These plots show an interesting effect appearing at high center-of-mass energies, namely the spin transfer to the  $\bar{\Lambda}$  decreases its sensitivity to the parton distributions. In fact, the spin transfer to  $\Lambda$  hyperons shows a similar trend as in case of the COMPASS kinematics with a lower center-of-mass energy (see Fig. 8), while  $\bar{\Lambda}$  hyperons are apparently not as sensitive as one might naively expect. This effect can be understood as follows. At high center-of-mass energies the charged leptons scatter preferentially on sea quarks and antiquarks, and quite often the hadronic string is produced between a quark and antiquark pair from the nucleon sea (in contrast to the case of lower center-of-mass energy, where the hadronic string is typically produced between a scattered valence quark and remnant diquark). This explains the peak around zero in the  $x_F$  distribution of the produced hadrons (as seen in Fig. 3). The majority of  $\bar{\Lambda}$  hyperons is produced from the fragmentation of the color string stretched between a  $u - \bar{u}$  (or  $d - \bar{d}$ ) pair with an increasing contribution from  $s - \bar{s}$  at larger  $x_F$ . However even those produced from the  $s - \bar{s}$  color string fragmentation often are far from the struck  $\bar{s}$  end and thus are not polarized. This explains the loss of sensitivity of spin transfer to  $\bar{\Lambda}$  hyperons to the  $\bar{s}(x)$  distribution at higher center-of-mass energies. On the other hand, the spin transfer to  $\Lambda$  hyperons is still sensitive to the  $s(x)$  distribution because there is an additional mechanism for producing  $\Lambda$  hyperons from the string stretched from the struck  $s$  quark target nucleon remnant (just as a  $s - ud$  string may produce a  $K^+$  or  $K^{*+}$  meson without fragmentation from  $u\bar{s}$  remnant quarks).

### 3.5 Comparison between the SU(6) and BJ Models for $\Lambda$ Spin Structure

We demonstrate now that accurate measurement of  $\bar{\Lambda}$  polarization could provide valuable information about  $\bar{\Lambda}$  spin structure.

In Fig. 10 the spin transfers to  $\Lambda$  and  $\bar{\Lambda}$  hyperons in the SU(6) (solid line) and BJ (dashed line) models as functions of  $x_F$  are shown for the case of COMPASS kinematics. A similar study is displayed in Fig. 11 for the case of HERA kinematics. It is apparent that the  $x_F > 0$  domain provides a clean tool for discriminating between the SU(6) and BJ models for both  $\Lambda$  and  $\bar{\Lambda}$  and for both COMPASS and HERA. On the other hand, as we noticed in Sec. 3.4, the HERA case for  $\bar{\Lambda}$  is not very sensitive to the  $\bar{s}$  parametrization, so a measurement of the spin transfer to  $\bar{\Lambda}$  at HERA would provide a complementary tool for separating the SU(6) and BJ models.

### 3.6 $\Lambda$ Spin Transfer and the Sea-Quark Polarization

We have demonstrated that at high energies the  $\bar{\Lambda}$  spin transfer is sensitive to the fragmentation of the antistrange quark. As we now show, it is also interesting that at low energies the  $\Lambda$  spin transfer could provide important information about the polarization of the sea quarks.

We have calculated the  $\Lambda$  spin transfer for DIS ( $Q^2 > 1 \text{ GeV}^2$ ) in typical JLAB conditions, assuming  $E_e = 5.7 \text{ GeV}$ .

At this energy the diquark contribution to  $\Lambda$  production dominates all the other possibilities, for all values of  $x_F$ . Therefore, in this case spin-transfer measurements offer an ideal opportunity to probe the diquark mechanism for spin transfer in which the polarization of the target remnant is due to the correlation between the polarizations of the struck quark and the sea quark defined in (3).

We show in Fig. 12 the predictions of our model for the spin transfer to the  $\Lambda$  hyperons in the SU(6) models for the GRV98 set of parton distributions, as functions of  $x$  and  $x_F$ . The solid line corresponds to the full calculation, whereas the amount of spin transfer without the contribution of the  $u, d$  quarks is shown as the thin dashed line, and the spin transfer without the contribution of the  $s$  quarks is shown as the dash-dotted line. The bold dashed line shows the spin transfer when we set  $C_{sq} = 0$  in (3). One can see that the spin transfer is not sensitive to the strange or light quark contributions. The main important contribution is due to strange sea-quark polarization. Switching off this contribution, i.e., assuming that  $C_{sq} = 0$ , leads to a significant change in the behaviour of the spin transfer to  $\Lambda$ .

## 4 Conclusions

We introduced in our previous work [25] theoretical and phenomenological studies of the spin transfers to  $\Lambda$  hyperons from various mechanisms in lepton-nucleon deep-inelastic scattering and presented model that described

adequately all the data available at that time on  $\Lambda$  polarization in (anti-) neutrino-nucleon and charged lepton-nucleon deep-inelastic scattering. The model had only two free parameters, which were fitted from NOMAD data [19]. In this paper we have extended and sharpened our predictions, introducing also the consideration of the spin transfer to  $\bar{\Lambda}$  hyperons produced in various deep-inelastic scattering processes. Our main predictions have been for the spin transfer to  $\Lambda$  and  $\bar{\Lambda}$  hyperons in the COMPASS experiment, which is taking data at the moment, and we have also provided predictions for the ongoing HERA electron-proton collider experiments H1 and ZEUS with longitudinally-polarized electrons, and for the spin transfer to  $\Lambda$  hyperons in a JLAB fixed-target experiment.

We have demonstrated that the accurate measurement of the spin transfers to  $\Lambda$  and  $\bar{\Lambda}$  hyperons with COMPASS kinematics has the potential to probe the intrinsic strangeness in the nucleon. We have shown that a measurement of  $\bar{\Lambda}$  polarization could provide a clean probe of the spin transfer from  $\bar{s}$  antiquarks. It provides a new possibility to measure the antistrange quark distribution function.

Finally, our results for a JLAB fixed target experiment indicate that spin transfer from the polarized electron beam to  $\Lambda$  hyperons, even produced on unpolarized proton target, would be dominated by the intrinsic polarized strangeness in the nucleon. Therefore, a measurement of  $\Lambda$  polarization at JLAB would provide a new cross-check of polarized intrinsic strangeness in the nucleon.

These studies have shown that the experimental opportunities available to COMPASS, HERA and JLAB are largely complementary. In combination, they could provide valuable information about polarization of the strange quarks in the nucleon.

We gratefully acknowledge V.Alexakhin, N.Vlasov and Liang Zuo-tang for useful discussions.

## References

1. S.Brodsky, J.Ellis, M.Karliner, *Phys.Lett.* **B206**, 309 (1988).
2. A.V.Efremov, O.V.Teryaev, *JINR preprint* **E2-88-287** (1988).
3. G.Altarelli, G.G.Ross, *Phys.Lett.* **B212**, 391 (1988).
4. R.D.Carlitz, J.C.Collins, A.H.Mueller, *Phys.Lett.* **B214**, 229 (1988).
5. S.Forte, *Phys.Lett.* **B224**, 189 (1989).
6. S.Forte, *Nucl.Phys.* **B331**, 1 (1990).
7. S.Forte, E.V.Shuryak, *Nucl.Phys.* **B357**, 153 (1991).
8. HERMES Collaboration, A.Airapetian et al., *Phys.Rev.Lett.* **84**, 2584 (2000).
9. SMC Collaboration, B.Adeva et al., *Phys.Rev.* **D70**, 012002 (2004).
10. COMPASS Collaboration, E.S.Ageev et al., *Phys.Lett.* **B633**, 25 (2006).
11. COMPASS Collaboration, G.K.Mallot, *Proc.17th International Spin Physics Symposium (SPIN06)*, Kyoto **arXiv:hep-ex/0612055** (2006).



12. M. Hirai, S. Kumano, N. Saito, *arXiv:hep-ph/0612037* (2006).
13. COMPASS Collaboration, V.Yu.Alexakhin et al., *Phys.Lett.* **B647**, 8 (2007).
14. E.Leader, A.V.Sidorov and D.B.Stamenov, *arXiv:hep-ph/0612360* (2006).
15. HERMES Collaboration, A.Airapetian et al., *arXiv:hep-ex/0609039* (2006).
16. HERMES Collaboration, A.Airapetian et al., *Phys.Rev.* **D71**, 012003 (2005).
17. A.M.Kotzinian, *Eur.Phys.J.* **C44**, 211 (2005).
18. J.Ellis, D.Kharzeev, A.M.Kotzinian, *Z.Phys.* **C69**, 467 (1996).
19. P. Astier et al., [NOMAD Collaboration], *Nucl.Phys.* **B588**, 3 (2000).
20. P. Astier et al. [NOMAD Collaboration], *Nucl.Phys.* **B605**, 3 (2001), hep-ex/0103047.
21. D. V. Naumov [NOMAD Collaboration], *Acta Phys.Polon.* **B33**, 3791 (2002), hep-ph/0206032.
22. D. V. Naumov [NOMAD Collaboration], *AIP Conf.Proc.* **570**, 489 (2001), hep-ph/0101325.
23. J.Ellis, M.Karliner, D.Kharzeev, M.G.Sapozhnikov, *Phys.Lett.* **B353**, 319 (1995).
24. J.Ellis, M.Karliner, D.Kharzeev, M.G.Sapozhnikov, *Nucl.Phys.* **A673**, 256 (2000).
25. J.Ellis, A.Kotzinian, D.Naumov, *Eur.Phys.J.* **C25**, 603–613 (2002).
26. M. Burkardt, and R. L. Jaffe, *Phys. Rev. Lett.* **70**, 2537 (1993).
27. M.Anselmino, M.Boglione, U.D'Alesio, E.Leader and F.Murgia, *Phys.Lett.* **B509**, 246 (2001).
28. A. M. Kotzinian, A. Bravar and D. von Harrach, *Eur.Phys.J.* **C2**, 329 (1998).
29. Chun-Xiu Liu, Qing-hua Xu and Zuo-tang Liang, *Phys.Rev.* **D64**, 073004 (2001).
30. Hui Dong, Jian Zhou, and Zuo-tang Liang, *Phys. Rev.* **D72**, 033006 (2005).
31. Chun-Xiu Liu, and Qing-hua Xu, and Zuo-tang Liang, *Int. J. Mod. Phys.* **A18**, 1485–1489 (2003).
32. Zuo-tang Liang, and Qing-hua Xu, *Phys. Rev.* **D65**, 113012 (2002).
33. Chun-Xiu Liu, and Zuo-tang Liang, *Phys. Rev.* **D62**, 094001 (2000).
34. Zuo-tang Liang, and Boros, C., *Phys. Rev. Lett.* **79**, 3608–3611 (1997).
35. J.-J. Yang, *Phys. Rev.* **D65**, 094035 (2002).
36. B. Ma, I. Schmidt, J. Soffer, and J. Yang, *Nucl. Phys.* **A703**, 346–364 (2002).
37. B. Ma, I. Schmidt, J. Soffer, and J. Yang, *Phys. Rev.* **D64**, 014017 (2001).
38. B. Ma, I. Schmidt, J. Soffer, and J. Yang, *Phys. Rev.* **D62**, 114009 (2000).
39. B. Ma, I. Schmidt, J. Soffer, and J. Yang, *Phys. Lett.* **B488**, 254–260 (2000).
40. D. de Florian, M. Stratmann, and W. Vogelsang, *Phys. Rev.* **D57**, 5811–5824 (1998).
41. D. Ashery, and H. J. Lipkin, *Phys. Lett.* **B469**, 263–269 (1999).
42. T. Sjöstrand, *Comp. Phys. Commun.* **39**, 347 (1986).
43. T. Sjöstrand, *Comp. Phys. Commun.* **43**, 367 (1987).
44. A. Chukanov (2006), PhD thesis, in Russian.
45. P. Astier et al. [NOMAD Collaboration], *Nucl.Phys.* **B621**, 3 (2002).

46. A. E. G. Ingelman, and J. Rathsman, *Comp. Phys. Commun.* **101**, 108 (1997).
47. H. Plochow-Besch., PDFLIB (2000), w5051.
48. COMPASS collaboration, M.G.Sapozhnikov, *Proceedings of XI Workshop on High Energy Spin Physics, SPIN-05, Dubna, September 2005*, *arXiv:hep-ex/0602002* (2006).
49. M. Gluck, E. Reya, A. Vogt, *Eur. Phys. J.* **C5**, 461 (1998).
50. F.Olness et al., *Eur.Phys.J.* **C 40**, 145 (2005), hep-ph/0312323.
51. CCFR and NuTeV Collaborations, M.Goncharov et al., *Phys.Rev.* **D64**, 112006 (2001).
52. NuTeV Collaboration, M.Tzanov et al. (2003), hep-ex/0306035.

## Figures

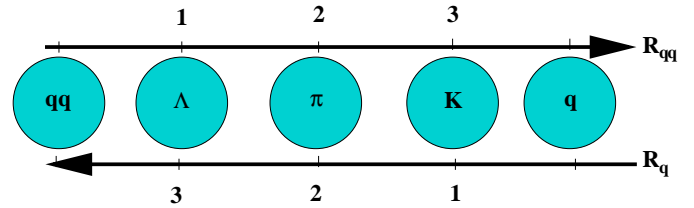


**Fig. 1.** The definitions of the two ranks  $R_q$  and  $R_{qq}$  that represent the numerical orderings from the quark and diquark ends of the Lund fragmentation string, respectively. In the example shown in this figure the  $\Lambda$  hyperon has  $R_{qq} = 1$  and  $R_q = 3$ , whereas the  $\pi$  has  $R_{qq} = R_q = 2$ .

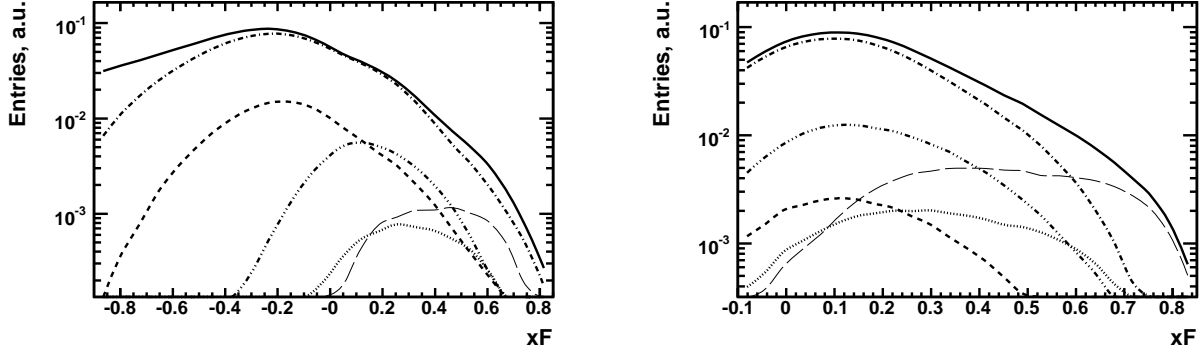


**Fig. 2.** Normalized  $x_F$  distributions of  $\Lambda$  (left) and  $\bar{\Lambda}$  (right) produced via different channels: long-dashed line - from  $s$  ( $\bar{s}$ ), dash-triple-dotted line - from  $u$  and  $d$  ( $\bar{d}$ ,  $\bar{u}$ ) light quarks, dash-dotted line - from the target nucleon end, dashed line - from decays of heavier resonances produced from the nucleon end of the string, dotted line - from decays of heavier resonances produced by quark fragmentation. These calculations were performed for the COMPASS energy in Model B using the GRV98 parametrization of the parton distribution functions and the SU(6) model of the baryon spin structure.

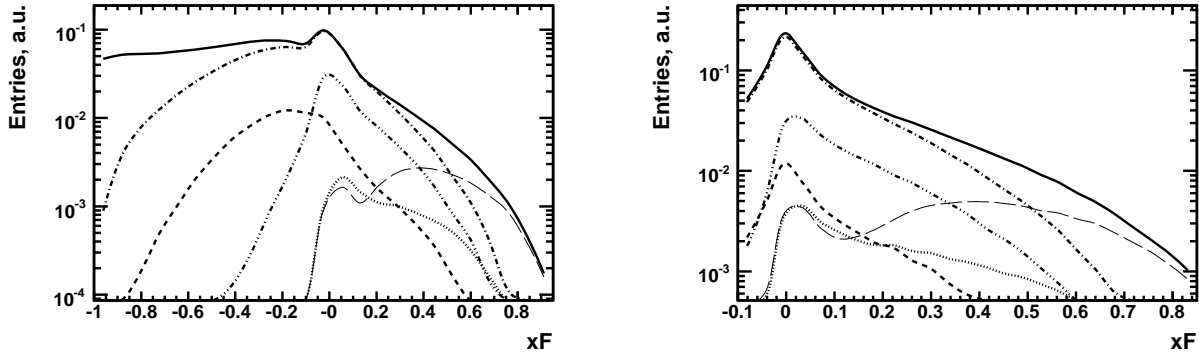


**Fig. 3.** Normalized  $x_F$  distributions of the  $\Lambda$  (left) and  $\bar{\Lambda}$  (right) produced at HERA energy via different channels: long-dashed line - from  $s$  ( $\bar{s}$ ), dash-triple-dotted line - from  $u$  and  $d$  ( $\bar{d}$ ,  $\bar{u}$ ) light quarks, dash-dotted line - from the target nucleon end, dashed line - from decays of heavier resonances produced from the nucleon end of the string, dotted line - from decays of heavier resonances produced by quark fragmentation. These calculations were performed in Model B using the GRV98 parametrization of the parton distribution functions and the SU(6) model of the baryon spin structure.

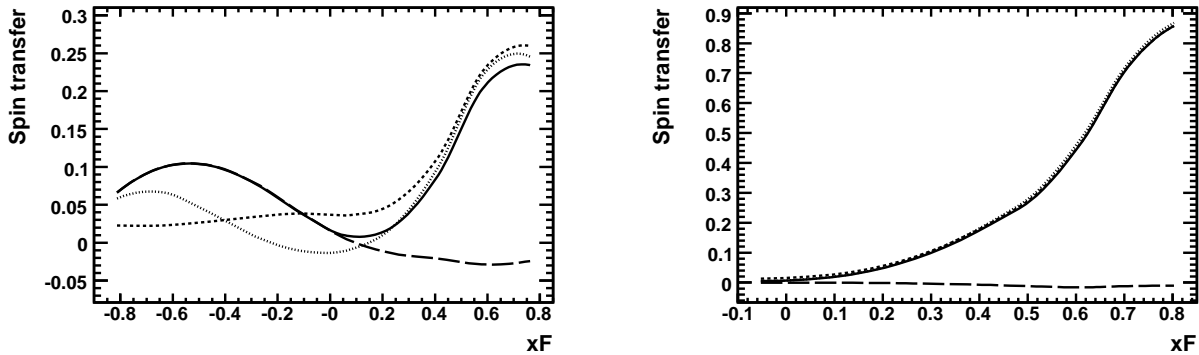


**Fig. 4.** The spin transfer to  $\Lambda$  hyperons (left) and  $\bar{\Lambda}$  hyperons (right) in the SU(6) variant of Model B, as a function of  $x_F$ , at COMPASS energy. The solid lines correspond to the full calculations, the spin transfers without the contributions from  $u$  and  $d$  quarks are shown by dotted lines, the spin transfers without the contributions from the  $s$  ( $\bar{s}$ ) struck quarks are shown by the long-dashed lines, and the dashed lines correspond to calculations with  $C_{sq} = 0$ .

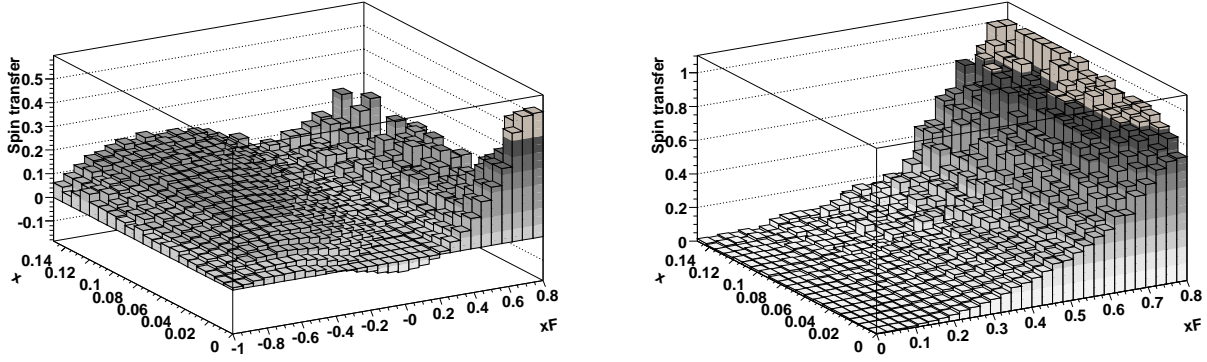


**Fig. 5.** The spin transfers to  $\Lambda$  (left) and  $\bar{\Lambda}$  hyperons (right) in the SU(6) variant of Model B, as functions of  $x_F$  and  $x$ , at COMPASS energy.

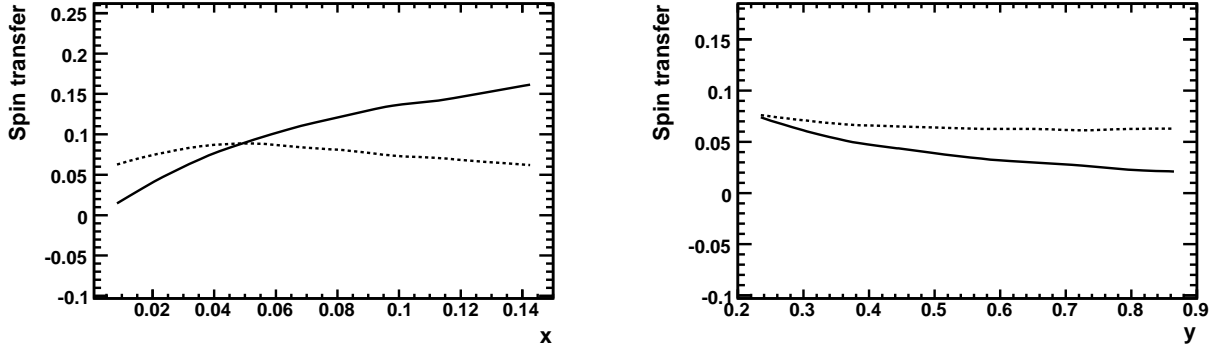


**Fig. 6.** The spin transfers to  $\Lambda$  (solid line) and  $\bar{\Lambda}$  (dashed line) hyperons in the SU(6) variant of Model B, as functions of  $x$  and  $y$ , at COMPASS energy.

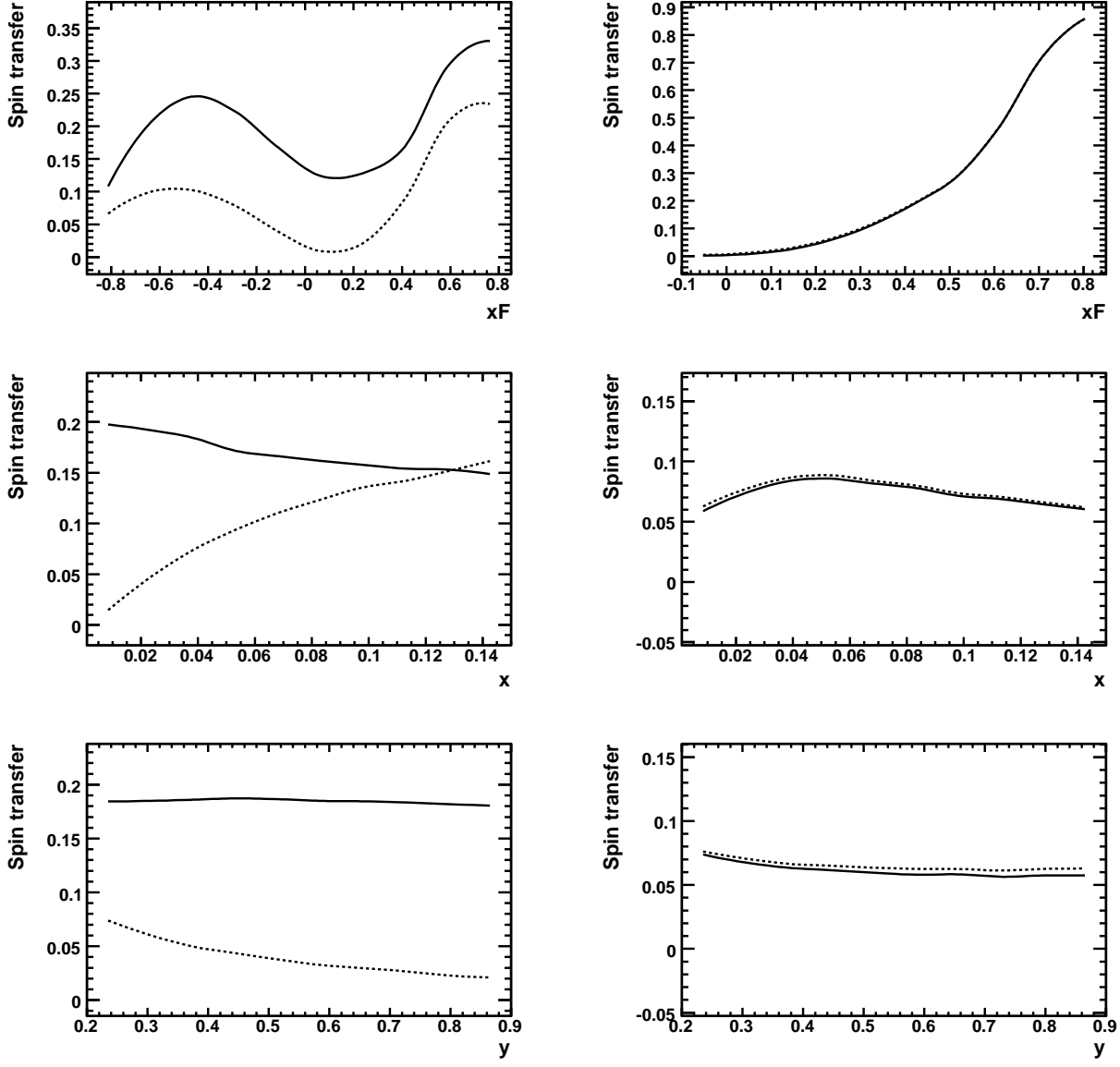


**Fig. 7.** Comparison of the spin-transfer predictions for Model A (solid line) and Model B (dashed line) for  $\Lambda$  (left) and  $\bar{\Lambda}$  (right) hyperons at COMPASS energy as functions of  $x$ ,  $x_F$  and  $y$ . We use the GRV98 parton distribution functions and the SU(6) model of the baryon spin structure.



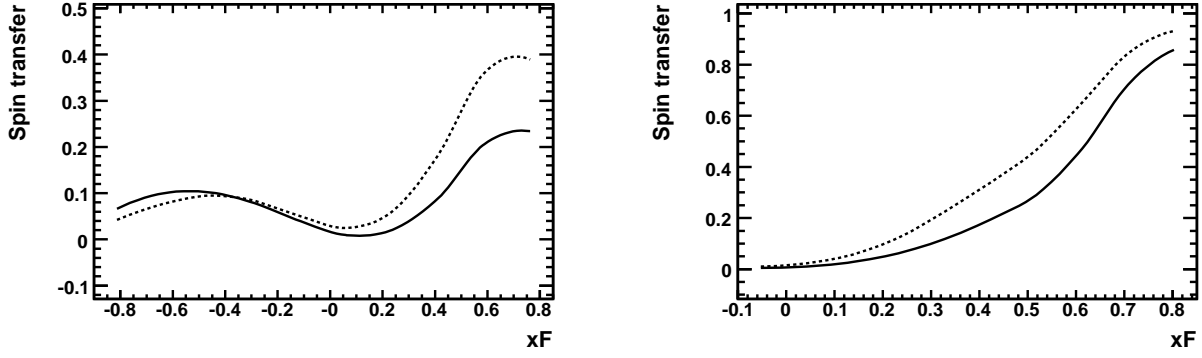


**Fig. 8.** The spin transfers to the  $\Lambda$  (left) and  $\bar{\Lambda}$  (right) hyperons in the SU(6) model for the GRV98 (solid line) and CTEQ5L (dashed line) sets of parton distributions, as functions of  $x_F$ , at COMPASS energy.

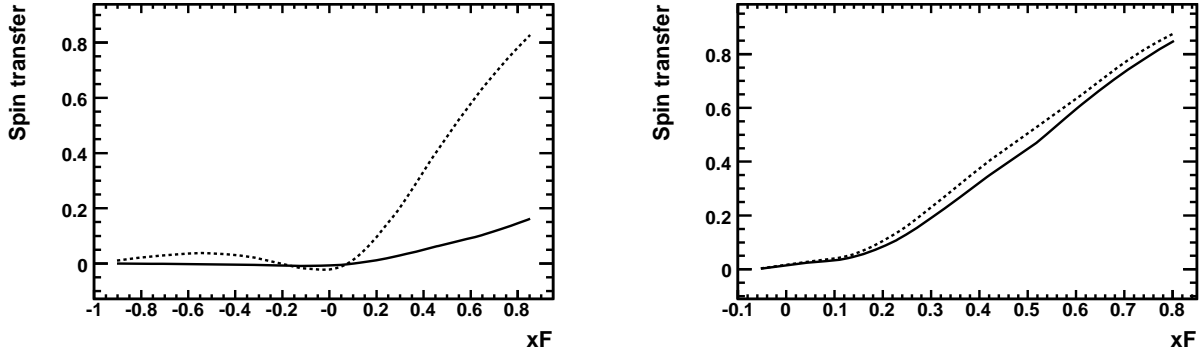


**Fig. 9.** The spin transfer to the  $\Lambda$  (left) and  $\bar{\Lambda}$  (right) hyperons in the SU(6) model for the GRV98 (solid line) and CTEQ5L (dashed line) sets of parton distributions, as functions of  $x_F$ , at HERA energy.

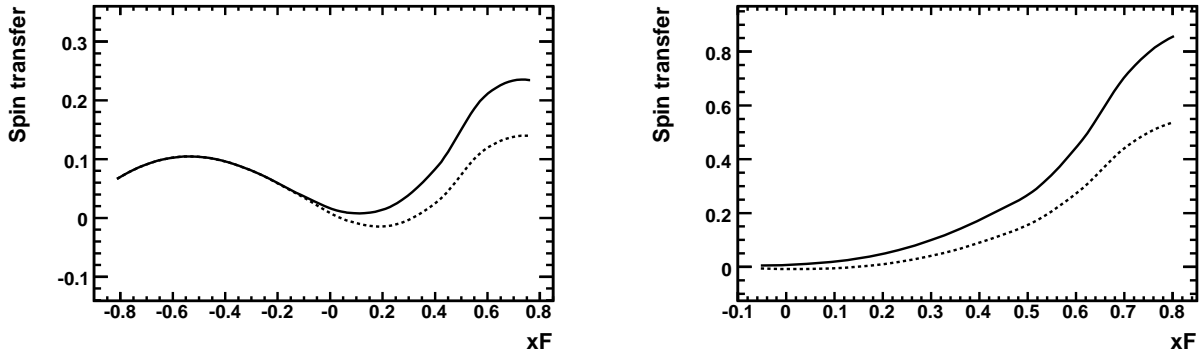


**Fig. 10.** The spin transfers to the  $\Lambda$  (left) and  $\bar{\Lambda}$  (right) hyperons in the SU(6) (solid line) and BJ (dashed line) models, assuming GRV98 parton distribution functions, as functions of  $x_F$ , at the COMPASS energy.

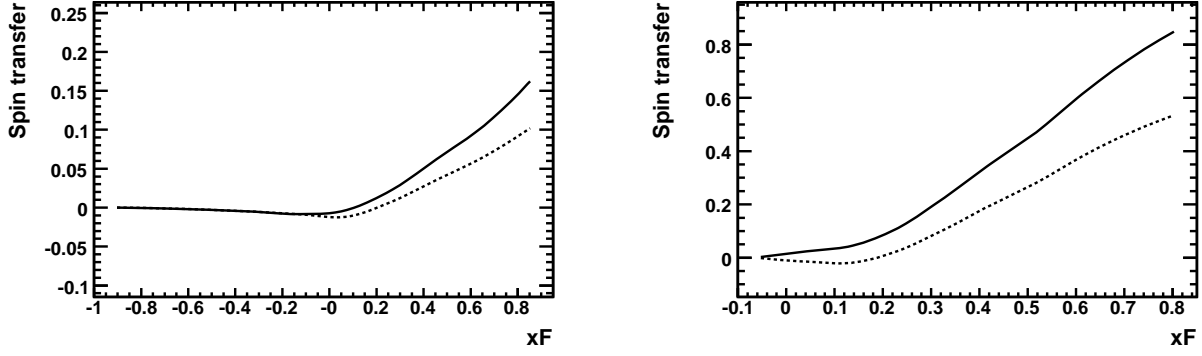


**Fig. 11.** The spin transfers to the  $\Lambda$  (left) and  $\bar{\Lambda}$  (right) hyperons in the SU(6) (solid line) and BJ (dashed line) models, assuming GRV98 parton distribution functions, as functions of  $x_F$ , at the HERA energy.

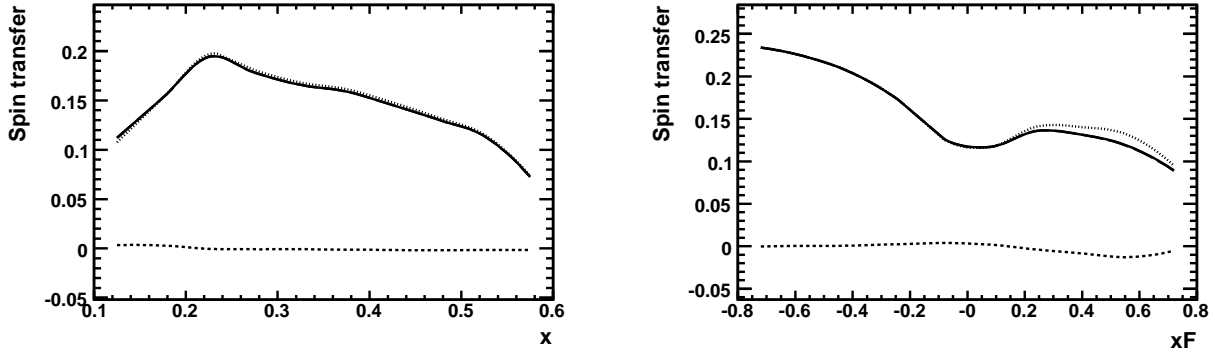


**Fig. 12.** The spin transfer to the  $\Lambda$  hyperons produced under JLAB experimental conditions in the SU(6) model for the GRV98 set of parton distributions, as functions of  $x$  (left) and  $x_F$  (right). The solid lines correspond to the full calculations, the spin transfers without the contributions from  $u$  and  $d$  quarks are shown by thin dashed lines, the spin transfers without the contributions from the  $s$  struck quarks are shown by the dash-dotted lines, and the bold dashed lines correspond to calculations with  $C_{sq} = 0$ .